Available online at www.sciencedirect.com
ScienceDirect
Computers and Geotechnics 35 (2008) 331–345
COMPUTERS AND GEOTECHNICS
www.elsevier.com/locate/compgeo

Inverse analysis techniques for parameter identification in simulation of excavation support systems

C. Rechea [a,*], S. Levasseur [b,1], R. Finno [c,2]

[a] SENER, Ingeniería y Sistemas, S.A. c/Severo Ochoa, 4 (P.T.M.), 28760 Tres Cantos, Madrid, Spain
[b] University Joseph Fourier – Grenoble I, Laboratory "Sols, Solides, Structures, Risques", CNRS UMR 5521, B.P. Box 53, 38041 Grenoble Cedex 9, France
[c] Department of Civil and Environmental Engineering, Northwestern University, Evanston, IL 60208, United States

Received 17 April 2007; received in revised form 20 July 2007; accepted 15 August 2007
Available online 24 October 2007

Abstract

Two numerical procedures are described that quantitatively identify a set of constitutive parameters that best represents observed ground movement data associated with deep excavations in urban environments. This inverse problem is solved by minimizing an objective (or error) function of the weighted least-squares type that contains the difference between observed and calculated ground displacements. The problem is solved with two different minimization algorithms, one based on a gradient method and the other on a genetic algorithm. The objective function is shown to be smooth with a unique solution. Both methods are applied to lateral movements from synthetic and real excavations to illustrate various aspects of the implementation of the methods. The advantages and disadvantages of each method applied to excavation problems are discussed.

Keywords: Excavation; Inverse problem; Genetic algorithm; Gradient method; Objective function; Parameter identification

1. Introduction

This paper describes two procedures to identify selected parameters of a soil constitutive model by inverse analysis of performance data from excavation support systems. The identification method is an iterative approach to solve the inverse problem [13,36]. Trial values of the unknown parameters are used as input values in a finite element code to simulate the associated direct problem until the discrepancies between measurements and numerical results are minimized. The problem is reduced to a parameter optimization.

Inverse analysis techniques have been applied to geotechnical problems since the 1980s (e.g., [13,4,33]). Their use allow one to evaluate performance of geotechnical structures by a quantifiable observational method. They have been used to identify soil parameters from laboratory or in situ tests [1,29,41,34], and performance data from excavation support systems [27,3,5,24], excavation of tunnels in rock [33,23,11,12,21,22], and embankment construction on soft soils [2,18,38]. Most of these previous studies of performance data were conducted with simple elastic or elasto-plastic soil models that severely restricted the ability of the computations to accurately reflect the observed field performance data, irrespective of employing inverse techniques.

When applying inverse analysis techniques to study the behavior of an actual supported excavation, concerns exist about the proper representation of the real system, as well as the efficiency of the inverse analysis technique and its ability to find a unique set of parameters for a particular problem. This paper focuses on the identification of soil parameters based on lateral movement data obtained close to the walls of excavation support systems.

* Corresponding author. Tel.: +34 918 077 323.
E-mail addresses: cecilia.rechea@sener.es (C. Rechea), severine.levasseur@hmg.inpg.fr (S. Levasseur), r-finno@northwestern.edu (R. Finno).
[1] Tel.: +33 0 4 76 82 51 83; fax: +33 0 4 76 82 70 00.
[2] Tel.: +1 847 491 5885.

0266-352X/$ - see front matter © 2007 Elsevier Ltd. All rights reserved.
doi:10.1016/j.compgeo.2007.08.008

Results from two optimization methods are presented, a gradient-based method developed by Hill [17] and applied to the excavation problem by Finno and Calvello [5] and a genetic algorithm method developed by Levasseur et al. [24]. The methods are applied to a "synthetic" excavation so as to evaluate each method without the complexity of real performance data and to a well-documented case study [6] to illustrate some of the judgment required to apply the methods in the field. In the former case, the field observations are artificially generated by FEM analyses and an optimal set of parameter values were chosen to reproduce representative orders of magnitude of measured performance data. This approach permits a direct comparison between the two inverse techniques without the interference of errors arising from simplifying the real geotechnical problem into a plane strain model, and field measurement errors other than those arising from instrument inaccuracies.

2. Background

Two main types of inverse analysis have been applied to geotechnics, optimization by iterative algorithms such as gradient methods [27,23,3,5,22] and optimization by techniques from the field of artificial intelligence, including artificial neural networks [40,16,15] or genetic algorithms [29,34,24]. These methods differ in their physical approach. The gradient method is a local parameter identification of a specific constitutive law. The artificial neural network is a method which creates by learning phases its own constitutive law from geotechnical measurements. Genetic algorithms are global optimization methods which localize an optimum set of solutions close to the "true" value.

Finno and Calvello [5] applied a gradient-based inverse analysis procedure to update predictions of lateral deformations observed during a 12.2 m deep excavation through Chicago glacial clays. The field observations were obtained from inclinometer data that measured lateral movements of the soil behind the supporting walls on opposite sides of the excavation throughout construction. The constitutive responses of the soil were represented by the Hardening-Soil (H-S) model [35]. Of the six basic H-S input parameters, only the reference value for the primary loading stiffness was optimized, while the other parameters were either kept constant or related to the updated value of the optimized value. Because the soil around the structure was already 'strained' due to previous construction activity at the site, the methodology could be effectively used to recalibrate the model of the excavation at early construction stages, such that good "predictions" could be made of the behavior of the soil at later stages. The final optimized parameters were reasonable and were within values that could have been reasonably selected *a priori*.

Levasseur et al. [24] discussed the use of inverse analysis by a genetic algorithm for the constitutive parameter identification of an *a priori* known soil constitutive law from typical geotechnical tests and measurements. In particular, parameters of the Mohr–Coulomb model were estimated to reproduce the horizontal displacements of a sheet pile wall between successive stages of excavation and also to reproduce the pressure–volume change responses from a pressuremeter test. The study showed genetic algorithms converge to a set of solutions close to the best one. The identified set of solutions characterized the soil properties well for a particular stress path. Furthermore, the evolution of the population process provided information about both parameter sensitivity and existing mathematical correlations between parameters. However, a drawback of genetic algorithm method can be its high calculation cost.

3. Procedures for inverse analysis

In this study, the commercial finite element program PLAXIS 8.2 was used to simulate the excavations in plane strain. The optimizations were carried out by coupling PLAXIS [30] with a search algorithm program and minimizing an objective function of the weighted least-squares type. Two different search algorithms were used and compared, a gradient method based in the Newton's method as published in the program UCODE [31], and a genetic search method developed by Laboratoire 3S-R for geotechnical studies [24].

3.1. Gradient method

UCODE is a universal inverse code that can be used with any application model. It performs inverse modeling posed as a parameter estimation problem, by calculating parameter values that minimize a weighted least-squares objective function using non-linear regression. Non-linear regression is needed when simulated values are non-linear with respect to parameters being estimated. The weighted least-squares objective function $S(\underline{b})$ is expressed as

$$S(\underline{b}) = [\underline{y} - \underline{y}'(\underline{b})]^{\mathrm{T}}\,\underline{\omega}[\underline{y} - \underline{y}'(\underline{b})] = \underline{e}^{\mathrm{T}}\,\underline{\omega e} \tag{1}$$

where $\underline{b}$ is a vector containing values of the parameters to be estimated; $\underline{y}$ the vector of the observations being matched by the regression; $\underline{y}'(\underline{b})$ the vector of the computed values which correspond to observations; $\underline{\omega}$ the weight matrix; and $\underline{e}$ the vector of residuals. This function represents a quantitative measure of the accuracy of the predictions.

In the inverse procedure, a sensitivity matrix $\underline{X}$, is computed using a forward difference approximation based on the changes in the computed solution due to slight perturbations of the estimated parameter values. Regression analysis of this non-linear problem is used to find the values of the parameters that result in a best fit between the computed and observed values. This fitting is accomplished with the Gauss–Newton method modified by the addition of a damping parameter and a Marquardt parameter [17].

The normal equations and the iterative process for the modified Gauss–Newton optimization method can be expressed as

$$(\underline{C}^{\mathrm{T}}\underline{X}_r^{\mathrm{T}}\underline{\omega}\underline{X}_r\underline{C} + \underline{I}m_r)\underline{C}^{-1}\underline{d}_r = \underline{C}^{\mathrm{T}}\underline{X}_r^{\mathrm{T}}\underline{\omega}(\underline{y} - \underline{y}'(\underline{b}_r)) \quad (2)$$

$$\underline{b}_{r+1} = \rho_r\underline{d}_r + \underline{b}_r \quad (3)$$

where r is the parameter estimation number; $\underline{X}_r$ the sensitivity matrix evaluated at parameter estimates $\underline{b}_r$ with elements equal to $\partial y'_i/\partial b_j$ calculated using forward or central differences; $\underline{\omega}$ the weight matrix; $\underline{X}_r^{\mathrm{T}}\underline{\omega}\underline{X}_r$ a symmetric, square matrix of NP by NP dimensions and NP the number of estimated parameters; $\underline{C}$ a diagonal scaling matrix with element c_{jj} equal to $\left[(\underline{X}^{\mathrm{T}}\underline{\omega}\underline{X})_{jj}\right]^{-1/2}$, which produces a scaled matrix with the smallest possible condition number [9,17]; $\underline{d}_r$ is a vector with the number of elements equal to the number of estimated parameters and it is used to update parameter estimates; $\underline{I}$ is an NP dimensional identity matrix; m_r is the Marquardt parameter [28]; and ρ_r is a damping parameter. The Marquardt parameter is used to improve regression performance for ill-posed problems. Initially $m_r = 0$ for each parameter estimation iteration r. For iterations in which the vector $\underline{d}$ defines parameter changes that are unlikely to reduce the value of the objective function, m_r is increased according to $m_r^{\mathrm{new}} = 1.5 \cdot m_r^{\mathrm{old}} + 0.001$ until the condition is no longer met.

The damping parameter, ρ_r, can vary in value from 0.0 to 1.0 and modifies all values in the parameter change vector $\underline{d}_r$ by the same factor. Thus, in vector terminology, the direction of $\underline{d}_r$ is preserved. The damping parameter is used to ensure that the absolute values of fractional parameter value changes are all less than a user-specified value, and to damp oscillations that occur when elements in $\underline{d}_r$ and $\underline{d}_{r-1}$ define opposite directions [17].

Non-linear regression begins with the initially estimated parameter values and ends when the parameter values change less than a fractional amount between regression iterations (0.01 for the Synthetic case and 0.05 for the Lurie Center case). When analyzing the Lurie case, an additional convergence criterion was imposed; therein, when the sum of the squared weighted residuals changed less than a fractional amount (0.05) over three regression iterations, the regression was stopped, indicating that model calibration was not progressing.

3.2. Genetic algorithm optimization method

The genetic algorithm (GA) is an optimization method inspired by Darwin's theory of evolution. It is a stochastic global search technique which does not need any derivative evaluation of the error function. It is recognized to be highly efficient in dealing with large, discrete, non-linear and poorly understood optimization problems [20,39]. This method does not guarantee the exact identification of the optimum solution of a problem. However, genetic mechanisms allow an optimum set of solutions to localize to the optimum in a given search space [10]. Its basic principles have been developed by Goldberg [14] and Renders [32]. The optimization program developed in Fortran language by Laboratoire 3S-R for geotechnical studies is based on this method [24].

The genetic algorithm objective (or error) function that assesses the discrepancy between the N measurements, Ue_i, and the associated numerical results, Un_i, is expressed as a scalar error function F_{err} in the sense of the least squares method:

$$F_{\mathrm{err}} = \left(\frac{1}{N}\sum_{i=1}^{N}\frac{(Ue_i - Un_i)^2}{\Delta U_i^2}\right)^{1/2} \quad (4)$$

$1/\Delta U_i$ is the weight given to the gap between Ue_i and Un_i. Physically, this parameter is linked to experimental and numerical uncertainties on point "i" and is expressed as

$$\Delta U_i = \varepsilon + \alpha Ue_i \quad (5)$$

where the parameter ε represents an absolute error of a measurement, and the parameter α represents a dimensionless relative error of a measurement. Through the values given to ε and α, one can change the description of uncertainties in the model.

The genetic algorithm optimization method consists of four main stages, including:

(1) *Defining the research space*: For N_p parameters to optimize, the minimization problem is solved in the N_p-dimension space, restricted to specified values for each parameter p between $p_{\min}$ and $p_{\max}$.
(2) *Encoding individuals and populations*: Each parameter is binary encoded with a given number of bytes (N_b) to form a gene. As this encoding meshes the research space into $(2^{Nb})^{Np}$ elements, the choice of N_b is directly linked to the expected precision of the parameter values. Concatenation of several genes forms an individual. Each individual represents one point of the research space, that is, a vector of solution parameters for a particular problem. A set of N_i individuals is a population. Note that the genetic algorithm is used on a meshed parameter research space. Consequently, the identified solutions are linked to the nodes of this mesh.
(3) *Generating an initial population*: A random set of N_i individuals, or initial population, is chosen within the research space. The objective function, or fitness F_{err}, of each individual of this population is evaluated by FEM calculation.
(4) *Selection*, *reproduction* and *mutation*: these mechanisms begin to evolve the population to better-adapted individuals of the research space.

Selection: Depending on the F_{err} values (minimal cost of the scalar error function), only the best $N_i/3$ individuals are preserved for the next population. These best individuals are called parents. This "elitist" selection is known to be more efficient for unimodal function optimization [14].

Reproduction and crossing: The parents are randomly paired off and crossed over to generate new pairs of individuals (see illustration in Table 1). To improve

Table 1
Illustration of the reproduction between a pair of parents to generate a new pair of individuals. The number of crossover points is nearly equal to the number of parameters. The positions of the crossover points are chosen at random

Parents	
Parent A:	1100 110 10011101 11100
Crossover points:	| | |
Parent B:	0110 001 01111011 00111
Reproduction	
Children 1 :	1100 001 10011101 00111
Crossover points :	| | |
Children 2 :	0110 110 01111011 11100

the algorithm efficiency the cross point number is chosen equal to the number of sought parameters [29]. This process is repeated until $2N_i/3$ new individuals, called children, are created.

Mutation and generation of a new population: Putting together the parent and the children individuals defines a new population of N_i individuals. To limit the convergence problems and to diversify the population, some of the individuals are randomly mutated (inversion of one byte on individual chain; see illustration in Table 2). Then, the objective function, F_{err}, of each individual of this new population is evaluated by FEM calculation.

These three last steps are repeated until one of the following convergence conditions are satisfied:

(i) if the average value of the error function applied to the parents or its standard deviation becomes small enough, the data are well reproduced by one or more parameter sets, specifically, a value of the error function less than 10^{-5} and 10^{-2} with standard deviations less than 10^{-6} and 10^{-3} for the Synthetic and Lurie Center excavation cases, respectively.
(ii) if the value of the error function applied to one individual becomes small compared to the others, then one solution is identified for the problem. In this case, either all the parents quickly converged to this individual or the convergence stopped after 20 iterations.

When the optimization is finished, a post-treatment analysis permits one to evaluate the solutions. The GA provides an optimum defined as the parameter values that give the minimal value of the scalar error function. However, because the GA converges without a guarantee to identify the exact optimum, these values are not necessary the exact sought parameters. The GA also yields several parameter combinations with an error function less than a given one, an error function less than 1.15 times the optimum one, and thus it defines a set of solutions for a problem. The average and the standard deviation of parameter values of this set permit one to evaluate a range of variation for each parameter value, and represents an approximation of the solution set.

Table 2
Illustration of mutation on individual

Individual before mutation	
Individual:	110000110 **0** 1110100111
Selected gene	|
Individual after mutation	
Muted individual:	110000110 **1** 1110100111
Muted gene	|

Both individual and byte, which are mutated, are chosen at random. The mutation probability P_{M} is about 2^{Np}.

4. Synthetic excavation

The purpose of these parametric studies of a synthetic excavation is to evaluate how well each algorithm reproduces the "field" displacements and to assure that parameters that do so with each model are indeed the "field" parameters that resulted in such movements. In other words, does each method converge to a "correct" solution? It is necessary to evaluate the numerics behind each procedure prior to applying the methods to field conditions because many more uncertainties exist when applying such procedures to real problems. A synthetic example allows a direct comparison of the two inverse analysis techniques without interference of model uncertainties and errors in field measurements other than those due to the precision of the instrumentation.

4.1. Description

The synthetic model is a 2-dimensional plane strain representation of a typical supported excavation through Chicago clays. The soil profile consists of 3.5 m of granular fill on top of a saturated clay layer of increasing strength and stiffness with depth. The retaining system is a 14 m deep sheet pile wall with two levels of internal bracing.

Fig. 1 shows the main features of this model. The excavated depth is 11 m. The model assumes perfect symmetry and only one-half of the excavation is represented. The soil response is assumed to follow that prescribed by the stress-level dependent, Hardening-Soil model [35].

4.2. Observations

The "field" data were generated by finite element analysis using selected input parameters noted as "field" parameters. The 'observations' employed here were computed soil horizontal displacements located along a vertical line 2 m behind the wall, a common location for an inclinometer in practice. The accuracy of a typical inclinometer is ± 2.4 mm/m, and this value was used herein. The errors associated with measurements were related to this accuracy, and this error is larger at the ground surface than at depth. In application, this implies that the weight matrix used in the gradient objective function Eq. (1) is diagonal. The weights were expressed as the inverse of the variance

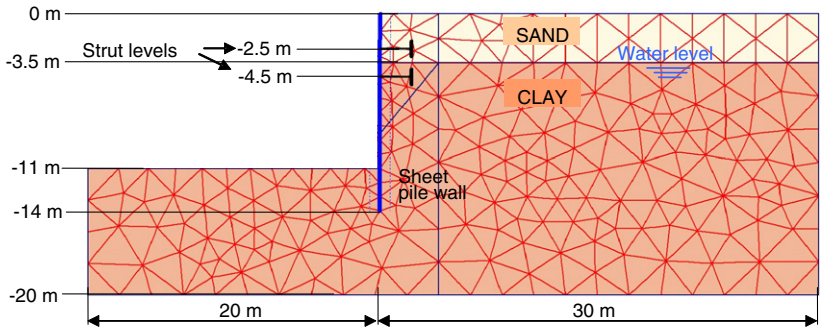

Fig. 1. Finite element model for synthetic case.

for the 95% confidence interval for the accuracy of the inclinometer. In the GA error function Eq. (5), the absolute error uncertainty ε is equal to zero and the relative error uncertainty α is equal to 2.4 mm/m. These considerations make the error structure different for each method.

For the gradient algorithm, the weighting of the observations is defined as

$$\omega_i(m^{-2}) = \frac{1}{\left(\frac{0.24}{1000 \cdot 1.96} \cdot d_i(m)\right)^2} \tag{6}$$

where d_i = distance to the bottom of the casing for the ith observation.

For the genetic algorithm, the weighting of the observations is defined as

$$\omega_i(m^{-2}) = \frac{1}{\left(\frac{0.24}{1000} \cdot Ue_i(m)\right)^2} \tag{7}$$

where Ue_i is the value of the ith observation. This definition of the weight makes the error in (7) about 4000 times smaller than the observation, and consequently no observations are excluded in the GA analyses.

4.3. Soil model, parameters and variations

The Hardening-Soil model is an elasto-plastic model for simulating the behavior of soils [35] and accounts for both volumetric and shear hardening. For volumetric hardening, an elliptical yield function is used and an associative flow rule is assumed. For shear hardening, a yield function of hyperbolic type is applied and a non-associative flow rule that incorporates a dilation angle is employed. Useful features of this model are its ability to represent the stress dependency of soil stiffness and to account for shear hardening, dilation and compression hardening. The model was chosen for this study because it resulted in good estimations of magnitude and vertical distribution of lateral ground movements close to the wall for the excavation at Chicago-State subway renovation project in Chicago [5].

Table 3 summarizes the Hardening-Soil model parameters employed as "field" values in the analysis. Of the nine parameters, only two in the clay layer were chosen for optimization. These are the reference values for primary deviatoric loading E_{50}^{ref}, and for elastic unloading–reloading E_{ur}^{ref}.

Table 3
Parameters for the Hardening-Soil model corresponding to the "field" observations. Synthetic case

Parameters	Sand layer	Clay layer
E_{50}^{ref} (kPa)	7200	[a]**20000**
E_{oed}^{ref} (kPa)	7200	14000
E_{ur}^{ref} (kPa)	21600	[a]**60000**
Power coefficient m	0.5	0.85
p^{ref} (kPa)	100	100
Cohesion c^{ref} (kPa)	0.2	0.2
Friction angle φ (°)	37	26
Dilatation angle ψ (°)	5	0
ν_{ur}	0.2	0.2

[a] Parameters for estimation.

They are the parameters that most influence the behavior of an excavation where movements are limited [5]. Values of the tangent stiffness for primary œdometer loading, E_{oed}^{ref}, were also varied in the analysis, but were always computed as 0.7 times the E_{50}^{ref} value on each iteration. The remaining parameters were given reasonable values according to data available for Chicago soils [8,5].

4.4. Results

The synthetic model was analyzed with both optimization methods. For the gradient method, five different parameter sets were considered – the "field" set of parameter values (the one that produces a zero value of the objective function), and four different sets of starting parameter values ranging from 1/4 to 4 times the "field" values. An added constraint arises because PLAXIS internally limits the values of parameter E_{ur}^{ref} between 2 and 20 times E_{50}^{ref}. For the genetic algorithm, two different tests were considered for optimization on a research space defined between 1/4 and 4 times the "field" values for the synthetic case. According to these limits for the research space, each parameter is encoded by 6 bytes for GA optimization. Then, the research space is composed of 2^6 times 2^6 nodes, or 4096 nodes. It imposes a mesh size for the research space equals to ±1170 kPa for E_{50}^{ref} and ±3500 kPa for E_{ur}^{ref}. For each optimization, the initial population is randomly defined on the research space. Because the genetic algorithm converges without a

Table 4
Results of convergence analyses for synthetic case

Gradient algorithm					Genetic algorithm		
Starting point	1/4 times "field" values	1/2 times "field" values	2 times "field" values	4 times "field" values	Test	1st test	2nd test
Initial E_{50}^{ref}	5000	10000	40000	80000	Research space	$E_{50}^{ref} \in [5000; 80000]$	
Initial E_{ur}^{ref}	15000	30000	120000	240000		$E_{ur}^{ref} \in [15000; 240000]$	
Optimum E_{50}^{ref}	20100	20000	20100	20000	Optimum E_{50}^{ref}	19100[a]	20200[a]
Optimum E_{ur}^{ref}	60000	60000	60000	60000	Optimum E_{ur}^{ref}	60700[a]	57200[a]
# of iterations	8	7	5	10	# of iterations	11	24
# PLAXIS runs	29	26	20	35	# PLAXIS runs	208	208
E_{50}^{ref} error	0.5%	0%	0.5%	0%	E_{50}^{ref} error	4.5%	1 %
E_{ur}^{ref} error	0%	0%	0%	0%	E_{ur}^{ref} error	1.2 %	4.7 %

"Field" values of E_{50}^{ref} and E_{ur}^{ref} are 20000 and 60000 kPa, respectively.
[a] "Mathematical" optimum for GA optimization.

guarantee to identify the exact optimum, a second GA optimization was conducted for this synthetic case to confirm the solution obtained by the first one, as suggested by Gallagher and Sambridge [10].

Table 4 presents the results obtained for all cases. For a synthetic case, the optimum is defined exactly. To simplify the comparison with the gradient method, the "mathematical" Genetic algorithm optima are considered for this synthetic case, corresponding to the parameter values with the minimal value of the GA error function. However, as the research space is meshed for GA optimization, we can notice that these GA results include uncertainties on parameter values equal to ±1170 kPa for E_{50}^{ref} and ±3500 kPa for E_{ur}^{ref}(these values correspond to the chosen research space mesh size).

Table 4 shows that the field values were reproduced quite well with both techniques. As expected, the field values are identified more accurately with the gradient algorithm. It also shows the computational effort, expressed as total number of runs of the finite element code to achieve the final values: the genetic algorithm needed 208 runs for each case, compared to 20–35 runs needed by the gradient algorithm. In the GA approach, one must perform many finite element calculations at the beginning of the optimization process to define the error function topology in the search space. This sweep, which is essential for the genetic algorithm efficiency, makes this method very expensive if there are only a few parameters to identify.

Fig. 2 shows a contour plot of the objective functions. To draw the contour lines, the objective function was computed from finite element analyses for each of 233 pairs of parameter values $[E_{50}^{ref}, E_{ur}^{ref}]$, with contours generated by kriging [19] using the commercial software SURFER based on the discrete values. The progress of the optimization in the gradient method is indicated by the iteration number and symbol showing the parameter pair at that iteration. From the two starting points at different ends of the parameter range, the paths reach the optimum values

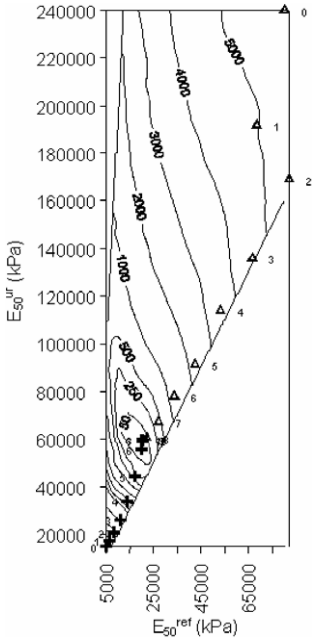

Fig. 2. Gradient algorithm. Contour of the weighted least-squares objective function in the $[E_{50}^{ref}, E_{ur}^{ref}]$ space and evolution of parameter estimation for starting points [80,000, 240,000] (△) and [5000, 20,000] (+). Optimum is [20,000, 60,000].

within 8–10 iterations. The contours show that the objective function is smooth with no secondary minima within this parameter space.

Fig. 3 shows the progress followed by the genetic algorithm. The shape of the objective function contours is similar to that computed by the gradient method and also exhibits one local minimum. Initially, the genetic algorithm evaluates the error function in 96 points chosen randomly on the research space with contours again found by kriging. This initial number of points corresponds to around 2% of all discrete parameter combinations for this space. Only the best third will remain in the next iteration and will generate children. By the first iteration, the genetic

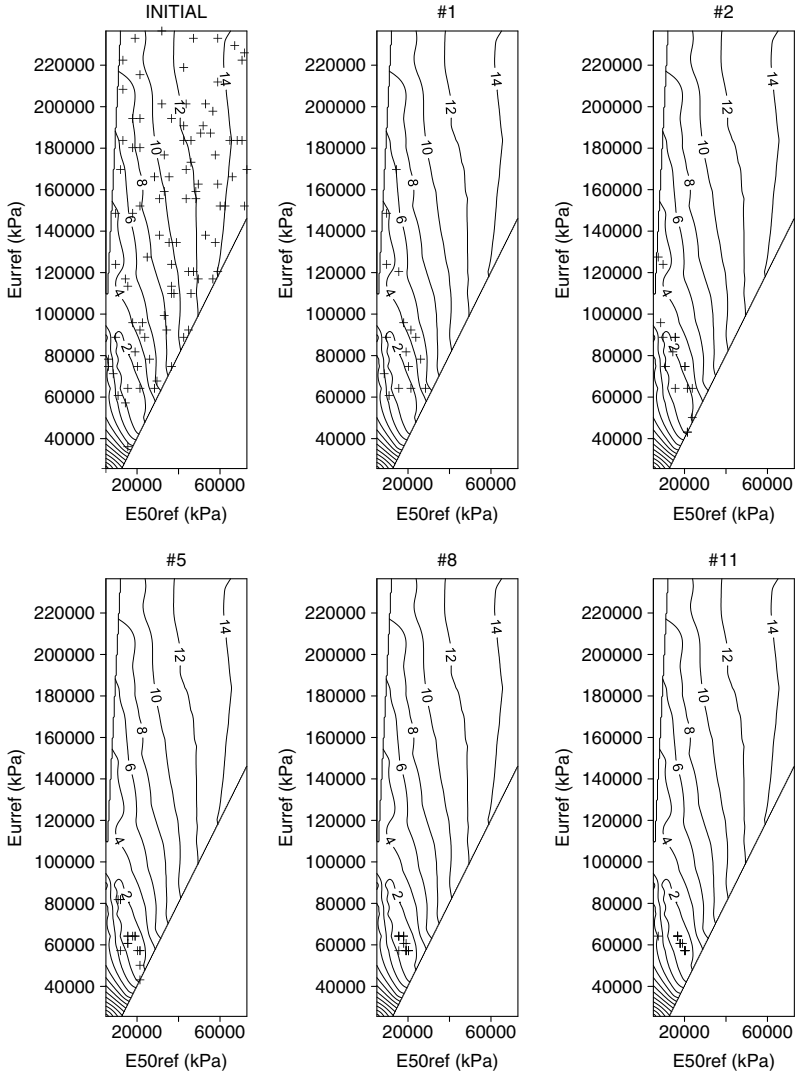

Fig. 3. Genetic algorithm. Contour of the error function in the $[E_{50}^{\mathrm{ref}}, E_{\mathrm{ur}}^{\mathrm{ref}}]$ space and evolution of parameter estimation. The value of the error function is multiplied by 10^4.

algorithm has quickly identified the better-adapted part on the research space in order to find the solution. Through the mechanism of selection, the less probable parameter sets are eliminated from the parent population. At the same time, crossings and mutations are used to create new individuals (not shown on this figure), in order to converge with more accuracy to the solution and to look for a possible other optimum on the research space. The genetic algorithm has reduced the search space to a very close area around the minimum after 11 iterations and converges to a "mathematical" minimum. All individuals of the parent population around the minimum could be considered as solution of the problem.

Fig. 4 compares the performance of the methods by plotting the fit improvement, FI, of the objective functions versus the iteration number, defined as

$$\mathrm{FI}_i = \frac{S(b)_{\mathrm{ini}} - S(b)_i}{S(b)_{\mathrm{ini}}} \tag{8}$$

where $S(b)_{\mathrm{ini}}$ is the initial value of the objective function and $S(b)_i$ is the optimized value of the objective function at the end of stage i. It indicates by what percentage the optimized results improved compared to the initial estimate. The figure shows that the genetic algorithm already has an 80% improvement only in the first iteration, whereas the gradient algorithm achieves between 15% and 60%, depending on how far the starting point is from the optimum.

Both methods yielded satisfactory results by reasonably estimating the "exact" parameter values. The gradient algorithm was more precise due to tight convergence criteria. The genetic algorithm yielded less accurate parameters because it is a global optimization method based on a meshed research space. The gradient method was much faster in achieving convergence, needing about 10 times fewer finite element iterations than the genetic algorithm. However, the genetic algorithm was capable of identifying a small region containing the optimum by the first iteration,

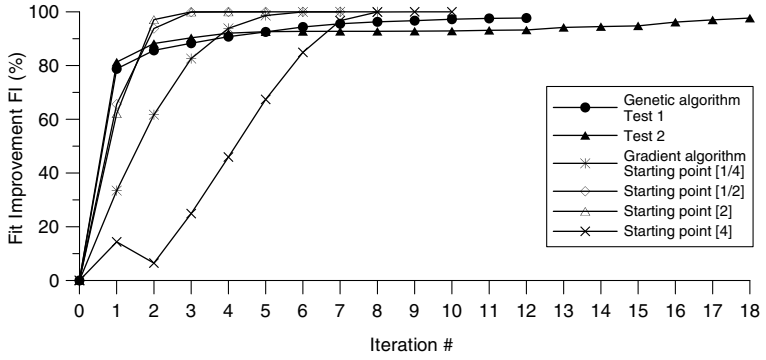

Fig. 4. Fit improvement versus iteration number for Genetic and Gradient algorithms.

with a fit improvement of 80%. The synthetic case shows that if the problem is well defined with few parameters to optimize, a gradient method is more efficient than the genetic algorithm method. It gives more precise results with less calculation. Intuitively, one would expect that GA is more suited for the simultaneous identification and optimization of many parameters. This aspect is discussed in more detail by Levasseur et al. [24].

5. Application to Lurie Research Center excavation

The two optimization techniques are applied to actual performance data that adds additional important constraints to the methods when dealing with field data. The purpose of this presentation is to evaluate if the algorithms will converge to a minimum value. Further, it illustrates issues related to the resolution of the inverse problem of this excavation (and likely many others as well) from the actual problem into a plane strain numerical simulation. This challenge exists in all excavation problems since the construction process is inherently 3-dimensional. This excavation was represented in 2D, assuming the center portion of the walls were adequately idealized as plane strain throughout the excavation process, so as the plane strain ratio equaled 1 [7,25,26] throughout construction. Ou defined the plane strain ratio PSR as the ratio of maximum lateral displacement calculated in three-dimensions, δ_{3D}, to the maximum lateral displacement calculated in plane strain, δ_{2D}. The field observations were selected such that they complied with those conditions, and were larger than measurement errors. With these two conditions, a meaningful estimation is theoretically possible.

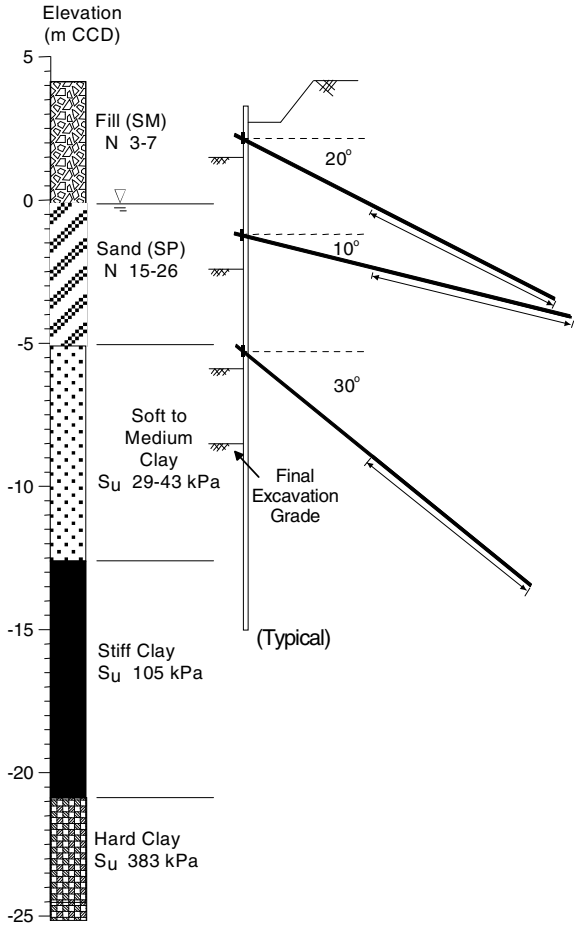

Fig. 5. Lurie Center excavation profile [6].

5.1. Description

The Lurie Research Center is located in downtown Chicago, IL. Plan dimensions of the excavation are 80 m by 68 m. This excavation and its observed performance were described in detail by Finno and Roboski [6].

Fig. 5 summarizes the soil profile at the site. Beneath the surficial medium dense to dense rubble fill lies a loose to medium dense beach sand. These granular soils overlie a sequence of glacial clays of increasing shear strength with depth. Undrained shear strengths, *Su*, in the soft to stiff clays in Fig. 5 are based on results of vane shear tests. The excavation averaged approximately 12.8 m deep and bottomed out in the medium stiff clay. The ground water level perched in the granular soils is related to the water level of the nearby Lake Michigan and it was located at approximately 0 m Chicago City Datum (CCD).

The retaining system consisted on a PZ-27 sheet pile wall on all sides. Two levels of tieback ground anchors were installed on the east wall due to the presence of the

basement of an adjacent building. Three levels of tieback anchors provided lateral support on the other three walls. Both the first and second level ground anchors were founded in the beach sand at approximately the same elevations. Because these two levels of anchors were staggered in the direction along the sheet pile wall, the spacing between the ground anchors was adequate to install them such that the performance tests were passed without resorting to post-grouting. This oddity in geometry affects the finite element model of the excavation, as will be discussed later.

Table 5
Major construction activities in Lurie site [6]

Stage number	Activity
1	Potholing and sheet-pile wall installation
2	Excavate to +1.52 m CCD and install and prestress first level of ground anchors at +2.13 m CCD
3	Construct caissons from working grade of +1.52 m CCD
4	Excavate to −2.44 m CCD and install and prestress second level of ground anchors at −1.22 m CCD
5	Excavate to −5.79 m CCD and install and prestress third level of ground anchors at −5.18 m CCD
6	Excavate to −8.53 m CCD and pour grade beams
7	Construct basement walls, pour slab and backfill

5.2. Field observations

The monitoring program consisted on eight inclinometers and 150 surface survey points, all put in place prior to wall installation. Fig. 6 shows the instrumentation layout. Finno and Roboski [6] defined seven major construction activities that could be correlated to performance data, as summarized in Table 5. Fig. 7 shows two of the inclinometer responses to these major construction activities. The data were re-zeroed after wall installation because in the finite element model for this problem the walls are wished-in-place and installation effects are not modeled.

Data from inclinometers LR8 on the south side, and the LR6 on the west side were selected to form the basis of the observations because the 3-dimensional stiffening effect of the corners did not affect significantly the data. This is important because the finite element model for the excavation was 2-dimensional. Finno and Roboski [6] showed that these locations remained close to a fully plane strain condition throughout excavation. Inclinometers from neither the north nor east sides were selected because adequate 2-D simulations could not be made due to lack of information related to the nearby building in the east side, and the abandoned timber piles on the north side. They provided restraint to movements that could not be represented in a

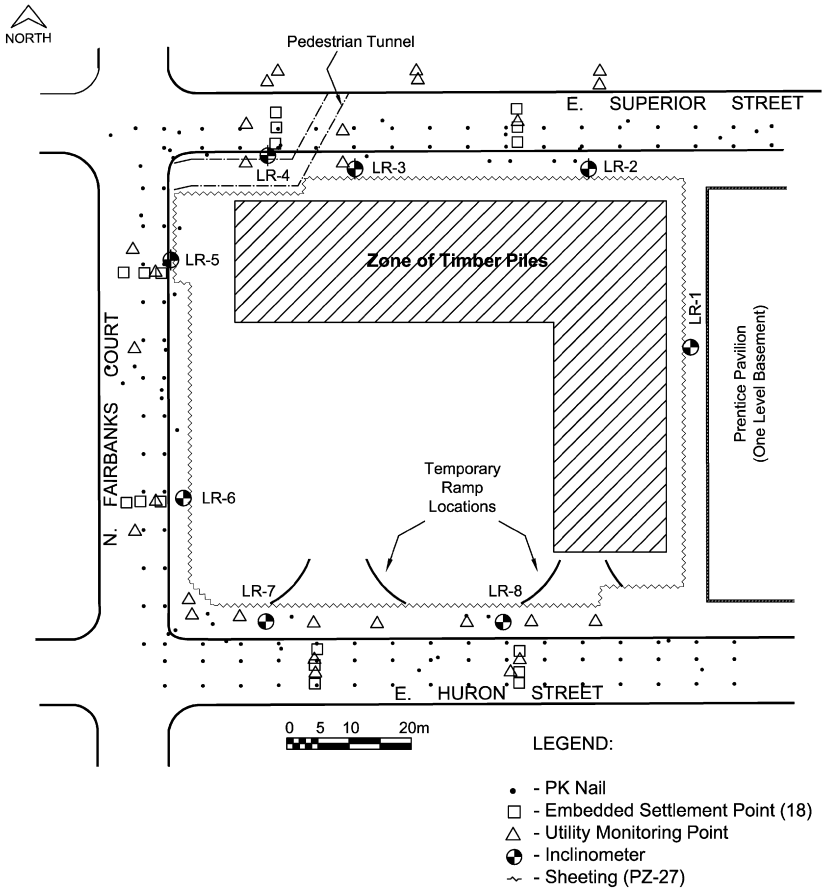

Fig. 6. Plan view and instrumentation layout in Lurie Center [6].

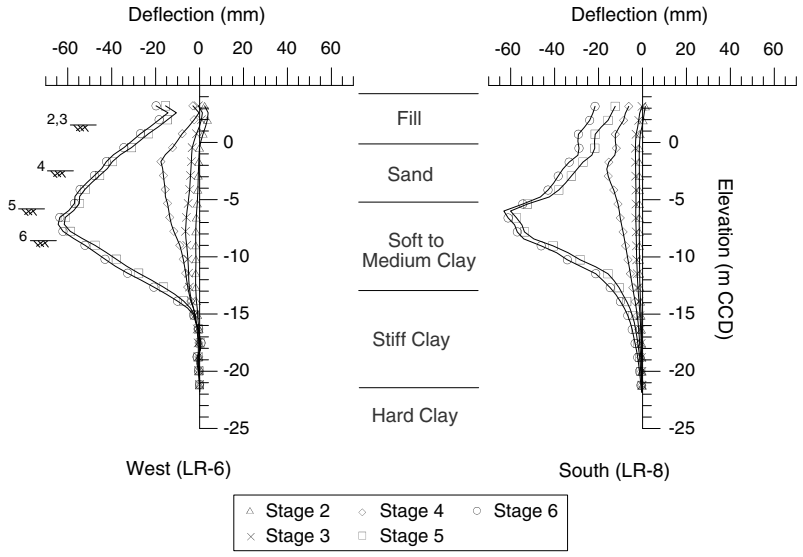

Fig. 7. Inclinometer response to mayor construction stages [6].

2-D simulation without creating more uncertainty about the effective soil parameters at those locations.

Fig. 7 shows that the lateral displacements remain relatively small during the first four stages. A sudden increase was observed when the excavation reaches 80 cm into the soft-medium clay for the installation of the third tieback level. This behavior was observed in all inclinometers. Also, inclinometer LR8 recorded maximum movements in the order of 10 mm in the stiff clay, while the inclinometer LR6 remains almost fixed at that same depth (elevations −12 to −15 m). Data from the geotechnical report for the stiff and hard clays suggested spatial variations in soil stiffness from east to west, with the soil stiffer in the west side.

The abrupt increase in measured displacements between construction stages 4 and 5 suggests that the soil strain levels before and after stage 5 are very different and so are the soil (stiffness) parameters that could be optimized. Recalibration of the model of the excavation at an early construction stage would not give, in this case, good "predictions" of the soil behavior at later stages because the variations in small strain stiffness are not included in the H-S model. Therefore, it was decided in this study that the optimizations would be carried out only for stage 6 to compare the two optimization approaches.

5.3. Finite element model

Fig. 8 shows the main features of the model at the south side of the excavation. Only one-half of the excavation is represented because the 68 m by 80 m excavation was wide and the support system, consisting of tiebacks, does not transfer forces from opposite sides, as it would occur if cross-lot bracing were used. The mesh extended 180 m away from the excavation, not entirely shown in the figure.

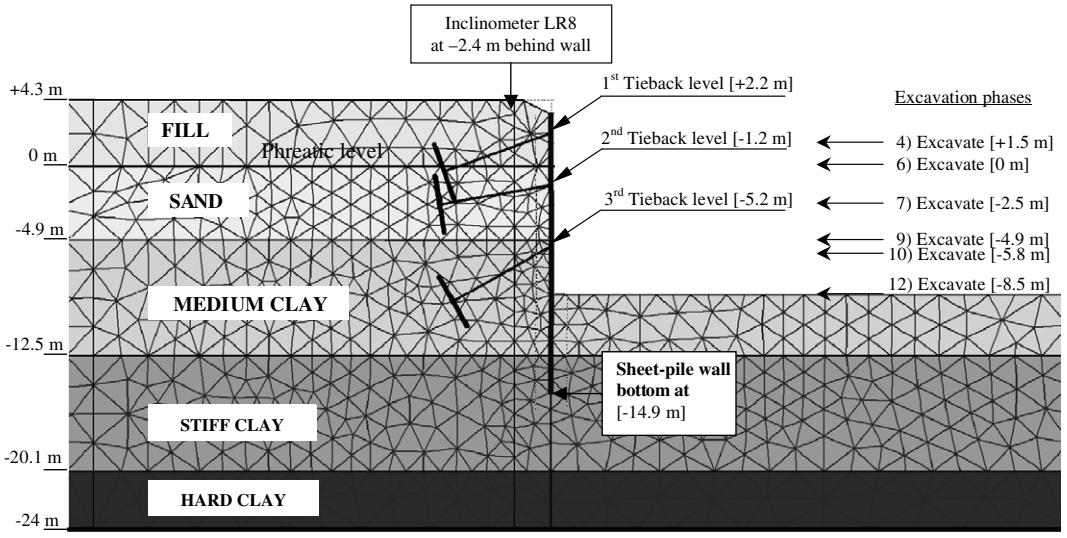

Fig. 8. Finite element model for Lurie excavation.

Table 6 summarizes the excavation stages as defined in the finite element model and their correspondence with the main construction activities. A key issue for representing this excavation in plane strain was the appropriate idealization of the tiebacks. The computed behavior of the upper soil was dominated by the way the tiebacks were represented, rather than by the constitutive responses of the fill and sand. This peculiarity arose because staggered anchors in the first two levels were represented in the plane strain simulation as being very close to one another without the benefit of the actual distance between them in the direction parallel to the wall, resulting in concentration of the stresses in the soil near the anchors and producing excessive lateral wall displacements. The field conditions were better approximated when the tiebacks were simulated as elastic struts oriented along the axis of the tiebacks.

5.4. Parameters and variations

The stress–strain behavior of all soil layers were modeled as Hardening soil responses. As shown in Table 7, the optimized soft-medium and stiff clay layer parameters were the reference value for the primary deviatoric loading, E_{50}^{ref}, in each layer. Inclinometer observations were taken only in these two layers. The reference value for the unloading–reloading elastic modulus, E_{ur}^{ref}, and the tangent stiffness for primary œdometer loading, E_{oed}^{ref}, were computed at each iteration as 3 and 0.7 times E_{50}^{ref}. The remaining parameters were defined following Finno and Calvello [5]. No settlement data were used as observations because the Hardening-Soil model does not reproduce well the settlement profile behind the wall, neither in magnitude nor shape. The version the Hardening-Soil model used in this work does not account for small strain non-linearity and thus could not represent the stiffness variation over the range of strain levels that diminishes with the distance to the wall.

Table 6
Excavation sequence as defined in PLAXIS for Lurie excavation

PLAXIS phase #	Correspondence with major construction activities (Table 5)	Description
0		Geostatic conditions
1		Reset displacements to zero at beginning of calculations Potholing
2		Refill
3	1	Wall installation
4		Reset displacements to zero after wall installation Excavate [+1.5 m CCD]
5	2	Prestress first level of tiebacks to 227.4 kN/m
6		Excavate [0 m CCD]
7		Lower water table to sand-clay interface at −4.9 CCD to simulate dewatering Excavate [−2.5 m CCD]
8	4	Prestress second level of tiebacks to 195 kN/m
9		Excavate [−4.9 m CCD]
10		Excavate [−5.8 m CCD]: Remove soil and water inside excavation while keeping undrained conditions in the non-excavated soil
11	5	Prestress third level of tiebacks to 340.4 kN/m
12	6	End excavation [−8.5 m CCD]: Remove soil and water inside excavation while keeping undrained conditions in the non-excavated soil

Table 7
Soil parameters for the Lurie Center model

Hardening-Soil parameters	Fill layer	Sand layer	Soft to medium clay layer	Stiff clay layer	Hard clay layer
Type	Drained	Drained	Undrained	Undrained	Undrained
E_{50}^{ref} (kPa)	13500	48000	*Studied parameter*	*Studied parameter*	$(1.5 \cdot E_{50}^{ref})_{Stiff}$
E_{ur}^{ref} (kPa)	13500	48000	$0.7 \cdot E_{50}^{ref}$	$0.7 \cdot E_{50}^{ref}$	$0.7 \cdot E_{50}^{ref}$
E_{oed}^{ref} (kPa)	40500	144000	$3 \cdot E_{50}^{ref}$	$3 \cdot E_{50}^{ref}$	$3 \cdot E_{50}^{ref}$
Power coefficient m	0.5	0.5	0.8	0.85	0.6
p^{ref} (kPa)	100	100	100	100	100
Cohesion c (kPa)	19	0.2	0.2	0.2	0.2
Friction angle φ (°)	30	35	26	32	25
Dilat. angle ψ (°)	2	5	0	0	0
v_{ur}	0.2	0.2	0.2	0.2	0.2
OCR	1	1.1	1.4	1.5	2.5

The research space for the application of the genetic algorithm was defined on the basis of the optimized parameter values from the Chicago-State case study [5]: $(E_{50}^{ref})_{medium\ clay} = 5000$ kPa and $(E_{50}^{ref})_{stiff\ clay} = 30,000$ kPa: the range varied between 1/3 and 3 times E_{50}^{ref} for the soft-medium clay, and between 1/6 and 6 times E_{50}^{ref} for the stiff clay. These ranges include parameter values based on inverse analyses of conventional drained triaxial compression tests conducted on tube samples extracted from the Chicago-State site. The research space is meshed in 64 by 64 elements that introduce uncertainties on the parameter estimates: ±350 kPa for E_{50}^{ref} in medium clay and ±2350 kPa for E_{50}^{ref} in stiff clay.

5.5. Selection of field observations

The observations used in the analysis were selected from inclinometers LR6 and LR8 readings at the end of the excavation (stage 6). They were taken below elevation −4.9 m CCD, within the clay layers. In practice, not all available observations could be used, but only those whose magnitudes were larger than their measurement errors, according to the definition of measurement error for the gradient method. This excluded half of the observations from inclinometer LR6 in the Stiff and Hard clays. Fig. 9 shows the field data for each inclinometer; marked with open circles are those excluded from the analysis: those from the fill and sand layers, and those from the clay layers that were too small.

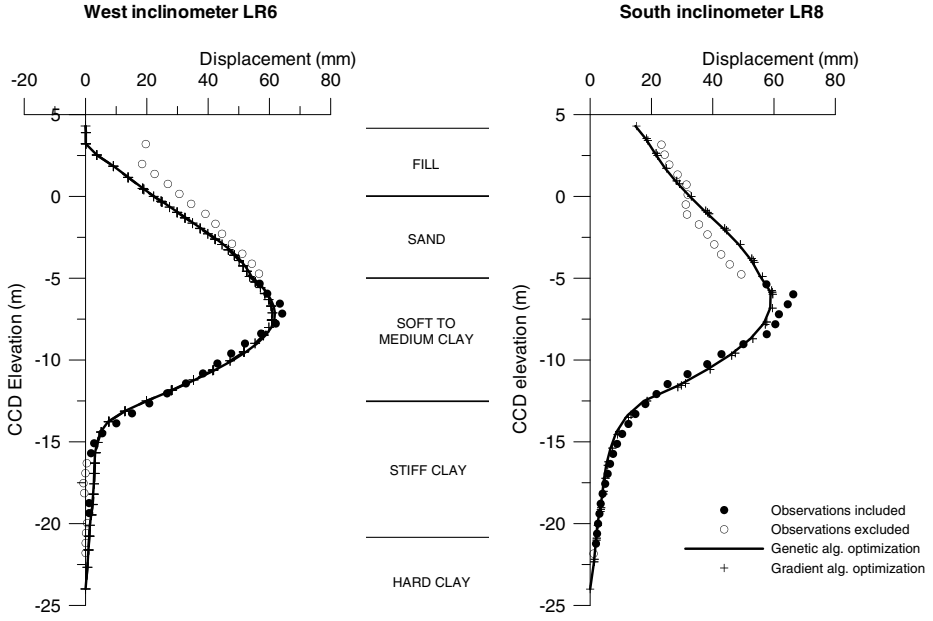

Fig. 9. Visual fit between observed and calculated displacements in Lurie.

5.6. Results

As with the Synthetic model, the Lurie Center excavation was analyzed with the two optimization methods. For each method, the objective and error functions are the same as those defined for the synthetic case.

Table 8 summarizes the results of the optimizations. There is little difference in the results generated by the two methods. Fig. 9 shows the computed and observed displacements based on the optimized parameters for each approach. Good agreement is seen for both cases. The optimized parameter value for the soft-medium clay shows little variation from method to method and between the south and the west models (4960–6020 kPa). This result indicates that the observations contain enough information for the parameter to be estimated accurately because the soft-medium clay layer is relatively deep, and contains enough observations with relatively large movements. Because of the lack of spatial difference in the results, the soft-medium clay is of relatively uniform composition across the site, as was also reflected in the site investigation data [6]. The good agreement between the computed and observed results also suggests that the selected cross-sections indeed responded in plane strain.

In contrast to the soft clay comparisons, only the LR8 readings contain enough information about the stiff clay for a meaningful parameter estimation. The estimated parameter value for the stiff clay is similar by both methods (52,200 and 56,250 kPa). For the inclinometer LR6 readings, the observations in the stiff clay are very small and of the same order of magnitude as the measurement error. The final estimates are similar for both methods (129,000 and 134,000 kPa) but there is some uncertainty in the estimation that can be appreciated in the contour

Table 8
Results of convergence analyses for Lurie center excavation

Gradient algorithm		West side LR6	South side LR8	Genetic algorithm		West side Incl. LR6	South side Incl. LR8
Initial values	$(E_{50}^{\mathrm{ref}})_{\mathrm{medium\ clay}}$	5000	5000	Research space	$(E_{50}^{ref})_{\mathrm{medium\ clay}}$	[2500; 25000]	
(kPa)	$(E_{50}^{\mathrm{ref}})_{\mathrm{stiff\ clay}}$	150000	50000	(kPa)	$(E_{50}^{\mathrm{ref}})_{\mathrm{stiff\ clay}}$	[50000; 200000]	
Final values	$(E_{50}^{\mathrm{ref}})_{\mathrm{medium\ clay}}$	**5060**	**6000**	Final values	$(E_{50}^{\mathrm{ref}})_{\mathrm{medium\ clay}}$	**4960**	**6020**
(kPa)	$(E_{50}^{\mathrm{ref}})_{\mathrm{stiff\ clay}}$	**129000**	**52200**	(kPa) (*)	$(E_{50}^{\mathrm{ref}})_{\mathrm{stiff\ clay}}$	**134000**	**56250**
				Final range for	$(E_{50}^{\mathrm{ref}})_{\mathrm{medium\ clay}}$	[4600; 5300]	[5650; 6350]
				parameters (**)	$(E_{50}^{\mathrm{ref}})_{\mathrm{stiff\ clay}}$	[124000; 164000]	[53000; 68000]
Final value $S(b)$		53	73	Final value F_{err}		0.37	0.46
# of iterations		2	2	# of iterations		9	22
# FEM calculations		11	11	# FEM calculations		167	179

(*) "Mathematical" GA optimum.
(**) "Statistical" GA parameter range of variation: calculated from parameters identified by GA with an error function less than $1.15F_{\mathrm{err}}$ final value.

plots of the objective functions in Fig. 10. These contours were based on 300 finite element simulations, each made with a different pair of the stiffness parameters. As can be seen, the objective functions are smooth and have a bounded solution in the research space considered. The contours in Fig. 10 are plotted using the data points generated with the error function, $S(b)$, defined for the gradient method, but those from the GA have similar shapes. The solution is better defined for the south side (LR8 measurements), with contour lines more concentrated around the optimum, as that location had more available observations and larger measured displacements in the Stiff clay layer than the west side. The contours of the objective function for the west side show a long narrow vertical valley, indicating that variations in values of E_{50}^{ref} *stiff* near optimum values of E_{50}^{ref} *med* have little impact on this solution, and thus are not well defined by the available observations.

For each method, a satisfactory optimum is obtained, with little difference between the optimized values. The differences in the final values computed by the two approaches are due to the different definition of the measurement error. Because those differences are small, the estimated parameter values are not very sensitive to the differences in the weights used in the two analyses. This result suggests that, in practice, accurate results can be obtained if the weighting is approximately correct. In this case the two error structures are similar and the error grows with the distance to the bottom of the casing (linearly for the gradient method, and proportionally to the observed values for the genetic algorithm).

In general, these results suggest that the problem has a unique solution in the research space considered. The gradient method and the genetic algorithm method reach basically the same parameter values. The solution is better defined for the south side, with its larger measured displacements in the stiff clay, than those measured on the west side.

6. Discussion

The set of field observations at the Lurie site was very complete, including inclinometer and settlement data at numerous locations and excavation stages, but they had to be carefully filtered because of model shortcomings. In addition to being a plane strain model, an important limitation is the constitutive model used to represent soil responses. The H-S model used herein does not take into account the variation of stiffness at very small strain levels, so settlement observations were not used as observations in any of the analyses. Also because of this same drawback, the optimized stiffness parameters would not be appropriate for the beginning stages of excavation where very small movements develop. Thus limitations arising from instrumentation accuracy and constitutive models limit the use of inverse analysis when trying to use field observations during early stages of excavation to predict what will occur during later stages, unless relatively large movements develop during early stages. This scenario occurred at the Chicago-State excavation [5] where 10 mm of lateral movement developed adjacent to a secant pile wall as it was installed.

The gradient method can identify an accurate solution to an inverse problem if the problem is well defined. Moreover, it needs less calculation cost than the genetic algorithm. Then, in this sense, the gradient method is more efficient than the GA method. However, the inverse analysis raises fundamental questions about the existence and

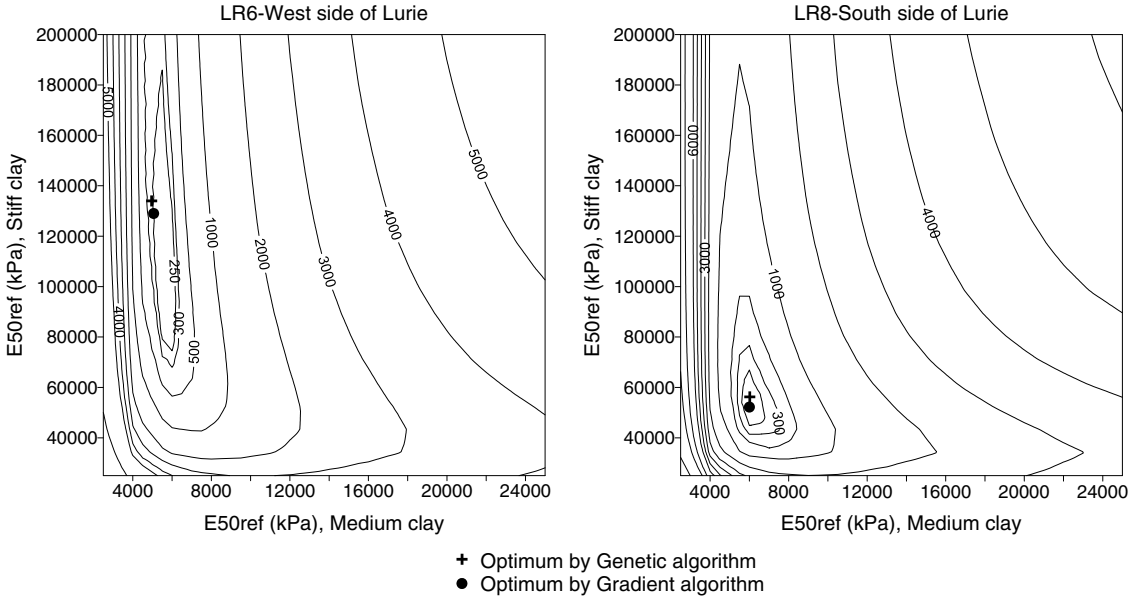

Fig. 10. Contours of the error functions, as computed by UCODE, and optima for Lurie case.

uniqueness of a solution [37]. Gradient optimization methods assume the solution of the inverse problem is unique. But inverse problems in the field of geotechnics using in situ measurements can be "ill-posed" unless care is taken in all aspects of the modeling, for example, expecting too much from a constitutive model or inadequately accounting for situ measurement uncertainties. In these cases, there is not one exact solution, but rather an infinite number of approximate solutions around an optimum. The aim of the parameter identification in this case should be the identification of the approximate solutions rather than the one with the arbitrarily-defined lowest error function. The GA permits the localization of an optimum set of solutions close to this optimum. In this sense, optimization by GA method in these cases is more relevant than gradient method.

7. Conclusions

Based on results of the inverse analyses of the Synthetic and the Lurie excavations by both gradient and genetic algorithm methods reported herein, the following conclusions can be drawn:

When both techniques were applied to a synthetic excavation, and two stiffness parameters from one clay layer were optimized, the results show that the problem had a unique solution even when the starting parameters were 1/4 to 4 times the actual "field" values. Both methods were accurate in the sense that the "field" parameters were obtained after optimization. The gradient method used less computational time to find the optimal solution. After one iteration, the GA method identified a small region that contained the optimum and the computed displacements had a fit improvement of 80%.

In the analysis of the Lurie excavation, one stiffness parameter in each of two clay layers was optimized. The optimization of this field case was unique in the research space considered. The search algorithms yielded similar results and the objective functions were smooth with no secondary minima. The solution was better defined on the side of the excavation with larger measured displacements in the stiff clay. When representing an excavation in plane strain, the simplification from 3D to 2D requires careful selection of observations from locations that are in fully plane strain condition for selected excavation stages and that are consistent with the predictive capabilities of the constitutive model selected to represent soil behavior.

Acknowledgements

Financial support for this work was provided by National Science Foundation grant CMS-0219123 and the Infrastructure Technology Institute (ITI) of Northwestern University. The support of Dr. Richard Fragaszy, program director at NSF, and Mr. David Schulz, ITI's director, is greatly appreciated. The writers would like to thank Y. Malécot, M. Boulon and E. Flavigny from the "Sols, Solides, Structures, Risques" laboratory, France, for their contributions in developing the GA optimization method.

References

[1] Anandarajah A, Agarwal D. Computer-aides calibration of soil plasticity model. Int J Numer Anal Meth Geomech 1991;15:835–56.
[2] Arai K, Ohta H, Kojima K. Application of back analysis to several test embankments on soft clay deposits. Soil Found 1986;26(2):60–72.
[3] Calvello M, Finno RJ. Selecting parameters to optimize in model calibration by inverse analysis. Comput Geotech 2004;31(5):411–25.
[4] Cividini A, Jurina L, Gioda G. Some aspects of characterization problems in geomechanics. Int J Rock Mech Min Sci Geomech Abstr 1981;18:487–503.
[5] Finno RJ, Calvello M. Supported excavations: observational method and inverse modeling. J Geotech Geoenviron Eng 2005;131(7): 826–36.
[6] Finno RJ, Roboski JF. Three-dimensional responses of a tied-back excavation through clay. J Geotech Geoenviron Eng 2005;131(3): 273–82.
[7] Finno RJ, Blackburn JT, Roboski JF. Three-dimensional effects for supported excavations in clay. J Geotech Geoenviron Eng, ASCE 2007;133(1):30–6.
[8] Finno RJ, Chung CK. Stress–strain-strength responses of compressible Chicago glacial clays. J Geotech Geoenviron Eng, ASCE 1992;118(10):1607–25.
[9] Forsythe GE, Strauss EG. On best conditioned matrices. Am Math Soc Proc 1955;10(3):340–5.
[10] Gallagher K, Sambridge M. Genetic algorithms: a powerful tool for large-scale nonlinear optimization problems. Comput Geosci 1994;20(7/8):1229–36.
[11] Gens A, Ledesma A, Alonso EE. Estimation of parameters in geotechnical backanalysis. 2. Application to a tunnel excavation problem. Comput Geotech 1996;18(1):29–46.
[12] Gioda G, Locatelli L. Back analysis of the measurements performed during the excavation of a shallow tunnel in sand. Int J Numer Anal Meth Geomech 1999;23:1407–25.
[13] Gioda G, Maier G. Direct search solution of an inverse problem in elastoplasticity: identification of cohesion, friction angle and in situ stress by pressure tunnel tests. Int J Numer Meth Eng 1980;15: 1823–48.
[14] Goldberg David E, editor. Genetic algorithms in search, optimization and machine learning. Adisson-Wesley; 1989.
[15] Hashash YMA, Marulanda C, Ghaboussi J, Jung S. Novel approach to integration of numerical modeling and field observation for deep excavation. J Geotech Geoenviron Eng 2006;132(8):1019–31.
[16] Hashash YMA, Marulanda C, Ghaboussi J, Jung S. Systematic update of deep excavation model using field performance data. Comput Geotech 2003;30:477–88.
[17] Hill M. Methods and guidelines for effective model calibration. US Geological Survey. Water-resources investigations report 98–4005; 1998.
[18] Honjo Y, Wen-Tsung L, Guha S. Inverse analysis of an embankment on soft clay by extended Bayesian method. Int J Numer Anal Meth Geomech 1994;18:709–34.
[19] Isaaks EH, Srivastava RM. An introduction to applied geoestatistics. New York: Oxford University Press; 1989.
[20] Kang YL, Lin XH, Qin QH. Inverse/genetic method and its application in identification of mechanical parameters of interface in composite. Compos Struct 2004;66:449–58.
[21] Lecampion B, Constantinescu A, Nguyen Minh D. Parameter identification for lined tunnels in viscoplastic medium. Int J Numer Anal Meth Geomech 2002;26:1191–211.
[22] Lecampion B, Contantinescu A. Sensitivity analysis for parameter identification in quasi-static poroelasticity. Int J Numer Anal Meth Geomech 2005;29:163–85.

[23] Ledesma A, Gens A, Alonso EE. Estimation of parameters in geotechnical backanalysis. I – Maximum likelihood approach. Comput Geotech 1996;18(1):1–27.
[24] Levasseur S, Malécot Y, Boulon M, Flavigny E. Soil parameter identification using a genetic algorithm. Int J Numer Anal Meth Geomech [in press].
[25] Ou CY, Chiou DC. Three-dimensional finite element analysis of deep excavations. In: Proceedings of the 11th Southeast Asian geotechnical congress, The Institute of Engineers, Malaysia, Kuala Lumpur, Malaysia; 1993. p. 769–74.
[26] Ou CY, Chiou DC, Wu TS. Three-dimensional finite element analysis of deep excavations. J Geotech Eng, ASCE 1996;122(5):473–83.
[27] Ou CY, Tang YG. Soil parameter determination for deep excavation analysis by optimization. J Chin Inst Eng 1994;17(5):671–88.
[28] Marquardt DW. An algorithm for least-squares estimation of nonlinear parameters. J Soc Ind Appl Math 1963;11(2):431–41.
[29] Pal S, Wathugala GW, Kundu S. Calibration of constitutive model using genetic algorithms. Comput Geotech 1996;19(4):325–48.
[30] PLAXIS. Finite element code for soil and rock analyses. http://www.plaxis.nl/ie.html.
[31] Poeter E, Hill M. UCODE, a computer code for universal inverse modeling. US geological survey; 1998.
[32] Renders J-M. Algorithmes génétiques et Réseaux de neurones. Hermès; 1994.
[33] Sakurai S, Takeuchi K. Back analysis of measured displacements of tunnels. Rock Mech Rock Eng 1983;16:173–80.
[34] Samarajiva P, Macari EJ, Wathugala W. Genetic algorithms for the calibration of constitutive models of soils. Int J Geomech 2005;5(3):206–17.
[35] Schantz T, Vermeer PA, Bonnier PG. Formulation and verification of the Hardening–Soil model. In: Brinkgreve RBJ, editor. Beyond 2000 in computational geotechnics. Balkema: Rotterdam; 1999. p. 281–90.
[36] Tarantola A. Inverse problem theory: methods for data fitting and model parameter estimation. Elsevier Science BV; 1987.
[37] Tikhonov A, Arsenine V. Solutions of ill-posed problems. Halsted Press; 1977.
[38] Wakita E, Matsuo M. Observational design method for earth structures constructed on soft ground. Géotechnique 1994;44(4):747–55.
[39] Wrobel L, Miltiadou P. Genetic algorithms for inverse cathodic protection problems. Eng Anal Bound Element 2004;28:267–77.
[40] Yamagami T, Jiang JC, Ueta Y. Back calculation of strength parameters for landslide control works using neural networks. In: Proceedings of the nineth international conference on computer methods and advances in geomechanics,Wuhan, China; 1997.
[41] Zentar R, Hicher PY, Moulin G. Identification of soil parameters by inverse analysis. Comput Geotech 2001;28:129–44.